View metadata, citation and similar papers at core.ac.uk

brought to you by CORE

provided by Dartmouth Digital Commons (Dartmouth College)

Dartmouth College

Dartmouth Digital Commons

Open Dartmouth: Peer-reviewed articles by Dartmouth faculty

Faculty Work

9-20-1999

Stellar Masses, Kinematics, and White Dwarf Composition for Three Close DA+dMe Binaries

Stephane Vennes
University of California - Berkeley

John R. Thorstensen
Dartmouth College

Elisha F. Polomski
University of Florida

Follow this and additional works at: https://digitalcommons.dartmouth.edu/facoa

 Part of the Stars, Interstellar Medium and the Galaxy Commons

Dartmouth Digital Commons Citation

Vennes, Stephane; Thorstensen, John R.; and Polomski, Elisha F., "Stellar Masses, Kinematics, and White Dwarf Composition for Three Close DA+dMe Binaries" (1999). *Open Dartmouth: Peer-reviewed articles by Dartmouth faculty*. 2277.
https://digitalcommons.dartmouth.edu/facoa/2277

This Article is brought to you for free and open access by the Faculty Work at Dartmouth Digital Commons. It has been accepted for inclusion in Open Dartmouth: Peer-reviewed articles by Dartmouth faculty by an authorized administrator of Dartmouth Digital Commons. For more information, please contact dartmouthdigitalcommons@groups.dartmouth.edu.

THE ASTROPHYSICAL JOURNAL, 523:386–398, 1999 September 20
© 1999. The American Astronomical Society. All rights reserved. Printed in U.S.A.

STELLAR MASSES, KINEMATICS, AND WHITE DWARF COMPOSITION FOR THREE CLOSE DA+dMe BINARIES

STÉPHANE VENNES
Astrophysical Theory Centre, Australian National University, ACT 0200, Australia; and Space Sciences Laboratory, University of California, Berkeley
JOHN R. THORSTENSEN
Department of Physics and Astronomy, Dartmouth College, Hanover, NH 03755
AND
ELISHA F. POLOMSKI
Department of Astronomy, 211 Bryant Space Science Center, University of Florida, Gainesville, FL 32611
Received 1998 December 28; accepted 1999 May 6

ABSTRACT

We determine the mass functions and mass ratios for three close white dwarf plus red dwarf binaries (EUVE J0720−317, 1016−053, and 2013+400). *Hubble Space Telescope* Goddard High-Resolution Spectrograph spectra of the He II λ1640 and C IV λ1550 spectral lines trace the white dwarf orbital motion, and Hamilton Spectrograph echelle spectra (Lick Observatory) and lower dispersion spectra trace the red dwarf orbital motion. The data sets allow us to measure orbital periods and velocities, as well as the white dwarf gravitational redshifts. The red dwarf and white dwarf mass estimates obtained from a combination of independent mass measurements for the white dwarf stars and our new orbital elements help constrain probable evolutionary outcomes. We find that EUVE J0720−317 will probably come into contact within a Hubble time and that the mass transfer will be unstable on a dynamical time. We also conclude that the much lower secondary masses in EUVE J1016−053 and EUVE J2013+400 exclude the possibility of significant interaction in these systems. We also present new helium and carbon photospheric abundance measurements in the three white dwarfs. The white dwarf atmospheric composition may show the effects of accretion of red dwarf mass-loss material onto its surface. Finally, we study the kinematics of the systems, and we also show that the white dwarf in EUVE J1016−053 is part of a quadruple system.

Subject headings: binaries: close — stars: abundances — ultraviolet: stars — white dwarfs

1. INTRODUCTION

Studies of post–common-envelope (CE) systems may help identify the initial conditions leading to the formation of cataclysmic variables. After it was realized that red giant radii often exceed binary orbital separations, Paczyński (1976) theorized that interactions between the red giant envelope and the secondary star (CE phase) result in dramatic orbital decay and frictional heating that contributes to the ejection of the envelope.Iben & Livio (1993) present a contemporary review of the problem. Empirical evidence of the phenomenon emerged with the discovery of a few evolved short-period binaries such as the K dwarf plus DA white dwarf system V471 Tau (Nelson & Young 1970) and the DA+dM system Feige 24 (Thorstensen et al. 1978). Several of these binaries are now known to populate the white dwarf cooling sequence, from young binaries such as Feige 24 (age $\leq 10^6$ yr) to much older objects (age $\geq 10^9$ yr). Ritter & Kolb (1998) present a comprehensive list of precataclysmic variables.

Accurate mass measurements are available for only a few systems. Based on such measurements, theory allows us to predict the timescale for orbital decay and, consequently, the period at which the secondary star initiates mass transfer (see King et al. 1994). Schmidt et al. (1995), for example, report mass measurements of the 4.17 hr DA2+dM3–5 binary GD 245 that suggest that the system will transfer material at a period of $P_{\rm con} = 2.7$ hr in $\sim 10^8$ yr. Another example of a bona fide precataclysmic variable is the DAO1+dM5–6 system NN Ser; based on their mass measurements, Catalán et al. (1994) estimate that the system will evolve into contact in $\sim 2 \times 10^9$ yr. However, many well-studied post-CE binaries have already experienced substantial orbital evolution, and a sample of young binaries would permit a more direct comparison between CE theory and observations. Magnetic braking and gravitational radiation considerably reduce the orbital period on timescales of 10^9 yr, and immediate post-CE characteristics gradually fade away. Samples of white dwarf stars selected at extreme ultraviolet (EUV) wavelengths enclose several *young* (age $\leq 10^6$ yr) post-CE systems that have probably not undergone significant orbital evolution (Vennes & Thorstensen 1994b, 1995). Apart from being selected solely on the basis of the white dwarf properties, i.e., thermal EUV emission, this post-CE sample is also part of a larger population of isolated white dwarfs with well-studied characteristics (see Vennes et al. 1997b). It should eventually be possible to scale the close-binary space density and birthrate from this extended population of white dwarfs.

The atmospheric composition of white dwarfs with close late-type companions is often peculiar and quite distinct from the composition of isolated white dwarfs of similar ages and masses. In particular, the detection of He II λ4686 in the close binary EUVE J1016−053 (RE 1016−053; Tweedy et al. 1993) suggests the effects of steady accretion of helium from the late-type star onto the white dwarf. Many young post-CE systems have a DAO white dwarf primary, i.e., of mixed hydrogen and helium composition. EUV spectra of the white dwarf in EUVE J1016−053 also show evidence of accreted heavy elements and EUV variability, which, coupled to the white dwarf rotation period,

indicate surface abundance inhomogeneities (Vennes et al. 1997a).

We have obtained high-dispersion optical and far-ultraviolet (FUV) spectroscopic observations of three EUV-selected post-CE binaries. This study is aimed at establishing the component masses and studying the chemical composition of the white dwarfs. We have also obtained low-dispersion optical spectra to refine the orbital ephemerides. The observations are presented in § 2 and the updated orbital elements are presented in § 3. Combining the dynamical mass measurements with spectroscopic mass (surface gravity) and gravitational redshift measurements, we determine the masses of the binary components (§ 4) and discuss evolutionary prospects in § 5. We examine the kinematical properties of the systems in § 6. Using FUV spectra of the white dwarfs we also constrain the helium and carbon abundances (§ 7); the measurements support a model of accretion of mass-loss material from the red dwarf onto the white dwarf. Finally, we summarize in § 8.

2. FUV AND OPTICAL SPECTROSCOPY

The successful analysis of *International Ultraviolet Explorer* (*IUE*) and KPNO echelle spectra of the 4.23 day DA+dM binary Feige 24 (Vennes & Thorstensen 1994a) incited us to attempt a similar experiment with the systems EUVE J0720−317, 1016−053, and 2013+400 (Table 1). Finder charts are available in Vennes & Thorstensen (1994b), Jomaron et al. (1993), and Thorstensen et al. (1994). The three new systems are more distant and fainter both in the optical and FUV spectral ranges. Moreover, the orbital periods are much shorter than in the case of Feige 24 ($\sim$1 vs. 4.23 days), and orbital smearing can be avoided only with relatively short spectroscopic exposures. We obtained the new high-dispersion spectroscopic observations using the *Hubble Space Telescope* (*HST*) Goddard High-Resolution Spectrograph (GHRS) and the Hamilton echelle spectrograph at Lick Observatory. We also improved the binary ephemerides with the acquisition of additional low-dispersion spectra at Michigan-Dartmouth-MIT (MDM) observatory, Lick Observatory, and Siding Spring Observatory (SSO).

2.1. *HST GHRS Spectroscopy*

In order to maximize the accuracy of the orbital velocity measurements, we scheduled the *HST* GHRS exposures close to orbital quadratures, i.e., in the phase ranges $\Phi = 0.15$–0.25 and $\Phi = 0.65$–0.75, using the well-established ephemerides of Thorstensen, Vennes, & Shambrook (1994), Thorstensen, Vennes, & Bowyer (1996), and Vennes & Thorstensen (1996). We used the G160M grating and the large science aperture. Wavelength calibrations are needed to determine the wavelength zero point accurately and subsequently calculate velocities; a WAVECAL exposure was performed with each new science exposure. The WAVECAL allows wavelength zero points to be determined to within 0.2 diodes. For the G160M grating, this allows wavelengths to be determined to within 0.0144 Å at worst. At 1550 Å this reduces the uncertainty in velocity from approximately 15 km s^{-1} (or a relative accuracy of 15% assuming a typical orbital velocity of 100 km s^{-1}) down to 3 km s^{-1} (3% accuracy). Figure 1 shows the normalized spectra obtained during this program. Note a weak C IV absorption component, possibly circumstellar, superposed upon the strong photospheric C IV doublet in EUVE J0720−317; similar circumstellar absorption was also noted toward Feige 24 (Dupree & Raymond 1982; Vennes & Thorstensen 1994a). Wavelength centroids were measured with the Gaussian fitting function in IRAF's "splot" routine. We used the Kelly (1987) wavelength tabulations of He II and C IV spectral lines and adopted the intensity average for He II (1640.430 Å). We have verified that pressure shifts do not affect the measured velocities significantly. For example, in a model appropriate for EUVE J0720−317, an optical depth of unity in the C IV line-forming region corresponds to an electron and proton density $n_e \sim n_p = 0.7$–1.1×10^{17} cm^{-3}. At such a density, Dimitrijevic, Sahal-Brechot, & Bommier (1991) predict a shift $v_p = -0.036$ to -0.055 km s^{-1}, an effect clearly unobservable. Table 2 shows the *HST* GHRS observation log and velocity measurements. The present measurements supersede past measurements based on low-dispersion spectroscopy of He II λ4686, which were possibly contaminated by chromospheric emission.

2.2. *Hamilton Echelle Spectroscopy and Radial Velocity Measurements*

Duplicating Vennes & Thorstensen's (1994a) study of Feige 24, we obtained, at Lick Observatory, a series of phase-resolved, high-dispersion spectra of EUVE J2013+400 on 1994 August 20–21 (UT), and of EUVE J0720−317 and EUVE J1016−053 on 1995 February 10–11 (UT). We used the 3 m telescope and the Hamilton echelle spectrograph equipped with a TI 800 × 800 CCD binned 2 × 2 for a dispersion of 0.055 Å pixel^{-1} at Hα. The slit width was set at 1.″5, resulting in a velocity resolution of $\sim$7 km s^{-1}. Figure 2 shows phase-resolved spectroscopy of

TABLE 1

SAMPLE OF CLOSE BINARIES

EUV/SOFT X-RAY CATALOGS					
2 EUVE J[a]	2 RE J[b]	1 RXS J[c]	DSS COORDINATES (2000)[d]	OTHER NAMES	V (mag)
0720−317.....	0720−314	072047.8−314705	07 20 47.9 −31 47 03	IN CMa	14.8
1016−053.....	1016−052	101628.3−052026	10 16 28.7 −05 20 34	...	14.1
2013+400.....	2013+400	201310.0+400222	20 13 09.2 +40 02 24	...	14.1

NOTE.—Units of right ascension are hours, minutes, and seconds, and units of declination are degrees, arcminutes, and arcseconds.

[a] From Bowyer et al. 1996.

[b] From Pye et al. 1995.

[c] From W. Voges, et al. 1996, available at http://www.rosat.mpe-garching.mpg.de/survey/rass-bsc/.

[d] Measured using Digitized Sky Survey plates (epoch circa 1980.

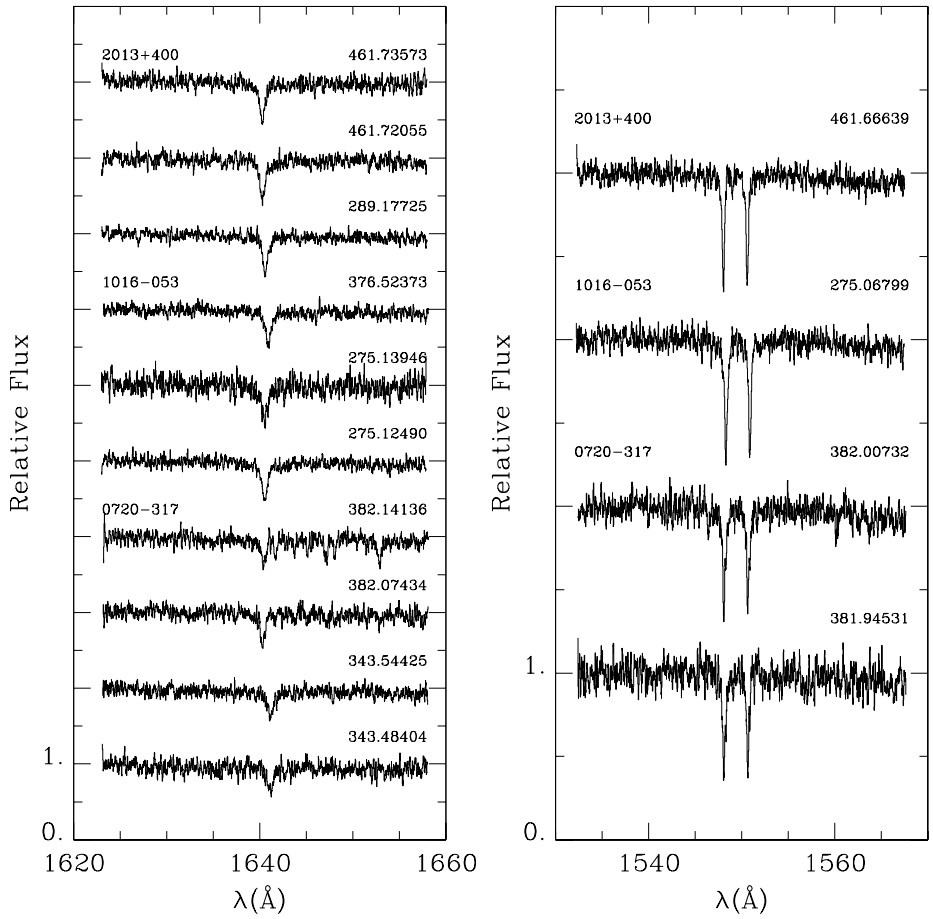

FIG. 1.—*HST* GHRS spectra of three hot white dwarfs in close binaries. Spectra from the same object are grouped together and labeled with HJD 2,450,000+. To maximize the accuracy of orbital velocity amplitudes, the He II λ1640 and C IV λ1550 spectra were obtained near orbital quadratures. Note a steady C IV absorption component toward EUVE J0720−317. Note also unidentified absorption lines in the spectrum of EUVE J0720−317 taken at HJD = 2,450,382.14136.

TABLE 2

HST OBSERVATION LOG

Mid-HJD (2,450,000+)	t_{exp} (s)	Spectral Range (Å)	Spectral Line	Phase	v (km s^{-1})
EUVE J0720−317					
343.48404.....	1714	1623–1658	He II λ1640.430	0.72762	+127.9
343.54425.....	2394	1623–1658	He II λ1640.430	0.77532	+131.6
381.94531.....	1714	1532–1568	C IV λ1548.202-1550.774	0.19320	−25.8
382.00732.....	2394	1532–1568	C IV λ1548.202-1550.774	0.24233	−27.7
382.07434.....	2394	1623–1658	He II λ1640.430	0.29541	−21.9
382.14136.....	2394	1623–1658	He II λ1640.430	0.34850	...[a]
EUVE J1016−053					
275.06799.....	1632	1532–1568	C IV λ1548.202-1550.774	0.17010	+17.8
275.12490.....	1795	1623–1658	He II λ1640.430	0.24221	+16.4
275.13946.....	544	1623–1658	He II λ1640.430	0.26065	+12.8
376.52373.....	1632	1623–1658	He II λ1640.430	0.71061	+87.7
EUVE J2013+400					
289.17725.....	1795	1623–1658	He II λ1640.430	0.74786	+27.4
461.66639.....	1795	1532–1568	C IV λ1548.202-1550.774	0.23437	−35.4
461.72055.....	1197	1623–1658	He II λ1640.430	0.31113	−25.6
461.73573.....	1251	1623–1658	He II λ1640.430	0.33265	−29.2

[a] He II λ1640 blended with unidentified features.

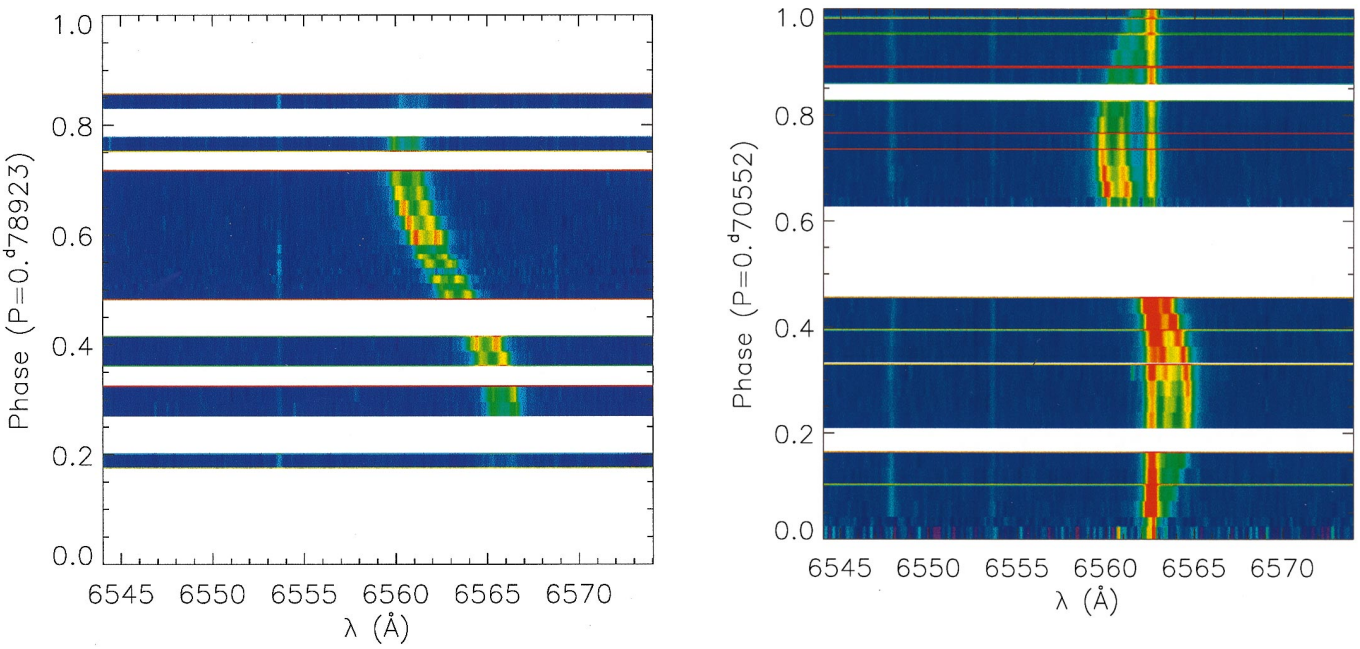

FIG. 2.—Hamilton echelle spectroscopy centered on Hα and displayed as a function of wavelength (Å) and orbital phase. The intensity scale is represented with the *IDL* red-green-blue scheme in decreasing order. Data gaps appear as blank rows. The Hα emission in EUVE J1016−053 (*left*) and EUVE J2013+400 (*right*) follows the red dwarf orbital motion and attains maximum intensity at superior conjunction ($\phi = 0.5$). The spectra of EUVE J1016−053 near superior conjunction are unfortunately contaminated by light from a crowding star, 3″.2 to the north. Note a steady nebular emission component in the spectra of EUVE J2013+400. Note also double-peaked emission in both objects.

EUVE J1016−053 and EUVE J2013+400. Note a stationary Hα nebular component in the line of sight toward EUVE J2013+400 (the red Palomar Observatory Sky Survey print shows considerable nebulosity in the area); we also obtained a sky exposure some 30″ west of EUVE J2013+400 that shows similar emission strength. Finally, we obtained a spectrum of the visual companion of EUVE J1016−053.

TABLE 3

LICK OBSERVATION LOG

HJD (2,449,000+)	$v_{H\alpha}$ (km s^{-1})	$v_{He\,I\,5875}$ (km s^{-1})	HJD (2,450,000+)	$v_{H\alpha}$ (km s^{-1})	$v_{He\,I\,5875}$ (km s^{-1})
		EUVE J1016−053			
770.70865.....	+149.3	+138.4	771.75367	+7.1	+15.4
770.78308.....	+155.6	+145.1	771.77571	−4.8	−11.5
770.80433.....	+150.0	+138.8	771.79810	−41.6	−33.5
770.85562.....	+119.1	+114.5	771.81938	−53.4	−47.8
770.87680.....	+104.7	+98.6	771.84067	−72.1	−64.8
770.89945.....	(+23.2)[a]		771.86192	−86.2	−78.2
770.95251.....	+21.8	+28.7	771.88318	−99.9	−90.4
770.97395.....	+10.0	+4.9	771.90460	−105.8	−97.2
770.99569.....	−19.6	−14.1	771.95460	−110.9	−103.2
771.01723.....	−45.6	−34.4	772.01569	−91.9	−81.7
		EUVE J2013+400			
585.70324.....	...	...	586.68823	...	...
585.71599.....	−102.7	−101.4	586.70101	−3.4	−2.1
585.73732.....	−109.9	−108.3	586.72237	+10.2	+13.1
585.75866.....	−113.8	−112.3	586.74391	+26.7	+28.8
585.78017.....	−114.9	−113.3	586.76522	+37.1	+37.6
585.80150.....	−113.2	−111.0	586.81894	+53.2	+53.0
585.82282.....	−108.6	−107.5	586.84024	+54.6	+54.5
585.86693.....	−88.7	−89.2	586.86156	+53.4	+53.5
585.89094.....	−68.9	−72.9	586.88288	+47.1	+49.6
585.91228.....	−54.6	−58.7	586.90623	+40.6	+40.6
585.93381.....	−42.5	−43.8	586.92754	+31.4	+30.8
585.95510.....	−29.3	−31.1	586.95025	+15.0	+17.6
586.66953.....	...	...	586.97175	+1.4	+2.6

[a] Observation of the visual companion.

In the Hamilton echelle data the emission lines were well resolved, and Hα showed a double-peaked structure (Fig. 2); we measured radial velocities by a convolution algorithm that emphasized the steep sides of the line profiles. In the case of EUVE J2013+400 we subtracted the off-source spectrum from the on-source spectra after scaling to minimize the contribution from the nebular component. We measured both the Hα and the He I λ5875 doublet (5875.62 and 5875.97 Å), for which we used the straight mean (5875.80 Å). Table 3 presents the Hamilton echelle observation log and velocity measurements.

2.3. *Intermediate-Resolution Spectroscopy and Radial Velocity Measurements*

We observed EUVE J2013+400 on 1994 August 22–23 using the 3 m telescope at Lick Observatory and the Kast double spectrograph equipped with a 452 line mm^{-1} grating on the blue side (2.54 Å $pixel^{-1}$ dispersion) and a 600 line mm^{-1} grating on the red side (2.32 Å $pixel^{-1}$ dispersion). The wavelength scale was established using HeAr (red side) and HeHgCd (blue side) comparison lamps. The slit width was set at 3″ for a spectral resolution of 6 Å. Additional spectra were obtained using the 2.4 m telescope at the MDM observatory on 1994 March and April and 1998 September with two different spectrographs. The MDM instrumentation used for this investigation is described in Thorstensen et al. (1994). Finally we observed EUVE J0720−317 and EUVE J1016−053 using the 2.3 m telescope at the SSO on 1998 June 17–18. We used the double spectrograph (DBS) equipped with a 300 lines mm^{-1} grating on the blue side (2.18 Å $pixel^{-1}$ dispersion) and a 316 lines mm^{-1} grating on the red side (2.08 Å $pixel^{-1}$ dispersion). We established the wavelength scale with NeAr (red side) and FeAr (blue side) comparison lamps. The slit width was set at 2″ for a spectral resolution of 5–6 Å. For intermediate resolution data (Kast, MDM, DBS) we measured velocities using convolution algorithms tuned to the narrow line cores (Schneider & Young 1980; Shafter 1983).

3. IMPROVED ORBITAL PERIODS AND EPHEMERIDES

We update the orbital periods originally presented by Thorstensen et al. (1994), Thorstensen et al. (1996), and Vennes & Thorstensen (1996) using new low- and high-dispersion spectroscopy. The new ephemerides allow us to determine with great accuracy the orbital phases at the time of the *HST* observations. The techniques used in searching for best periods are described in the previously cited work.

EUVE J0720−317.—The updated ephemeris, established over the time span of 1994 January through 1998 June, is

$$T = 2{,}449{,}696.192(9) + 1.26243(3)E\ , \qquad (1)$$

where T is the Julian date at which emission-line velocities increase through their mean value and E is an integer cycle count. The parentheses enclose formal 1 σ uncertainties in the last digits quoted.

EUVE J1016−053.—Our data now extend to 1998 June, and the total span of all available data (including that of Jomaron et al. 1993) is 2167 days. The updated ephemeris for EUVE J1016−053 is

$$T = 2{,}449{,}771.357(5) + 0.789278(12)E\ . \qquad (2)$$

EUVE J2013−400.—The period derived in Thorstensen et al. (1994) of $P = 0.7059 \pm 0.0003$ days was based on an unambiguous cycle count extending over 42 days. Our present data extend the range to 1807 days into 1998 September, again without ambiguity. Combining all data we establish the ephemeris for EUVE J2013+400:

$$T = 2{,}449{,}586.66122(58) + 0.705517(7)E\ , \qquad (3)$$

only 1.3 σ shorter than our previous estimates. The initial epoch is derived by combining fits to the Hamilton echelle data alone because of their very high precision, which defines the phase most accurately. Barstow et al. (1995a) find a period of 0.71013 ± 0.00020 days, which appears close to our period but which, in reality, differs by 23 of their quoted standard deviations. Because they claim their data uniquely define the period, there is a serious contradiction between our ephemerides and theirs. To investigate the problem, we ran a period search on the velocities given in their Table 4. The result demonstrates that unless they used other untabulated information, their sampling was actually insufficient to choose a unique period and they chose the wrong alias among many possibilities. Barstow et al.'s (1995a) ephemeris should be discarded.

TABLE 4

ORBITAL PARAMETERS

Parameter	EUVE J0720−317	EUVE J1016−053	EUVE J2013+400
Uncorrected Values			
P (days)	1.26243 ± 0.00003	0.78928 ± 0.00002	0.705519 ± 0.000006
K_{DA} (km s^{-1})	79.5 ± 1.4	37.5 ± 1.3	29.9 ± 2.5
K_{dMe} (km s^{-1})	101.8 ± 3.3	136.4 ± 1.4	84.2 ± 0.9
γ_{DA} (km s^{-1})	51.7 ± 1.3	51.9 ± 1.2	-1.9 ± 2.4
γ_{dMe} (km s^{-1})	29.0 ± 2.4	22.9 ± 0.9	-29.5 ± 0.7
γ_g (km s^{-1})	22.7 ± 2.6	29.0 ± 1.5	27.6 ± 2.4
q (M_{dMe}/M_{WD})	0.781 ± 0.039	0.275 ± 0.012	0.355 ± 0.031
$f(m_{WD})$ ($M_\odot$)	0.138 ± 0.013	0.208 ± 0.006	0.044 ± 0.001
Corrected Values[1]			
$K_{dMe,corr}$ (km s^{-1})	109.6 ± 5.6	140.9 ± 2.9	88.5 ± 1.6
q_{corr} (M_{dMe}/M_{WD})	0.725 ± 0.050	0.266 ± 0.015	0.338 ± 0.035
$f_{corr}(m_{WD})$ ($M_\odot$)	0.172 ± 0.026	0.229 ± 0.014	0.051 ± 0.003

[1] See § 4.

4. ORBITAL PARAMETERS AND STELLAR MASSES

Having established proper ephemerides, we now proceed with a complete analysis of the orbital elements. Note that we assume circular orbits, both because of theoretical expectations as well as because of prior analyses. We first measure the red dwarf and white dwarf velocity amplitudes and establish the mass ratio. Note that the Hα emission lines arise from the EUV-illuminated hemisphere and trace an orbit inferior to the red dwarf center of mass. A correction based on a simple geometrical model is proposed; the same correction may possibly underestimate the actual ratio of Feige 24's M-dwarf center-of-mass velocity amplitude, traced by absorption lines, to the velocity amplitude of Hα emission. Next we compute the white dwarf mass function, which, in combination with spectroscopic and gravitational redshift mass determinations, allows us to estimate probable system inclinations. The latter may serve as an input in attempts at modeling irradiation effects in these systems. Finally we infer a range of mass for the red dwarfs, which may then be compared with absolute luminosities and spectral types.

4.1. *Orbital Parameters*

Along with the ephemerides (§ 3) we also measured the red dwarf and white dwarf velocity amplitudes. Figure 3 shows our velocity measurements phased on the orbital periods for all three systems along with best fits (Table 4). We display accurate echelle velocities of the red dwarfs in EUVE J1016−053 and EUVE J2013+400 and all available low- and high-dispersion velocities of the red dwarf in EUVE J0720−317 (Vennes & Thorstensen 1996; this paper).

Vennes & Thorstensen (1994a) noted two important effects in their analysis of radial velocity measurements of Feige 24. First, they established a proper orbit for the M dwarf based on TiO absorption-band velocities and noted, as expected, that the emission-line velocities trace an orbit inferior to the center of mass: $K_{\rm TiO}/K_{\rm H\alpha} = 1.10 \pm 0.08$. Second, they noted a marginal offset between the systemic velocity based on absorption lines and the same velocity based on emission lines, $\gamma_{\rm TiO} - \gamma_{\rm H\alpha} = 3.9$ km s^{-1}, which they interpreted as evidence of chromospheric expansion. We apply the first correction to the red dwarf orbital velocity, but we exclude the correction to the systemic velocity, whose interpretation is not clear. A correction to the M dwarf orbital velocity may be obtained iteratively. A first estimate of the binary separation, a, is obtained using Kepler's law, the white dwarf spectroscopic mass, and the uncorrected mass ratio, q_0. We then estimate $a_{\rm dMe} = a(1+q)^{-1}$ and derive:

$$K_{\rm dMe,corr} = K_{\rm dMe} \times \left(1 - 0.4\,\frac{R_{\rm dMe}}{a_{\rm dMe}}\right)^{-1}, \qquad (4)$$

assuming $R_{\rm dMe}/R_\odot = (M_{\rm dMe}/M_\odot)^{0.7}$. The correction factor $a_{\rm dMe}/(a_{\rm dMe} - 0.4R_{\rm dMe})$ is the ratio of the red dwarf semimajor axis to the reduced red dwarf semimajor axis traced by the illuminated hemisphere, i.e., $a_{\rm dMe} - 0.4R_{\rm dMe}$, where $0.4R_{\rm dMe}$ is the distance from the center of the stellar disk to the center of the illuminated hemisphere. Applying this correction to the case of Feige 24 results in a predicted ratio $K_{\rm TiO}/K_{\rm H\alpha} = 1.017 \pm 0.005$, a value apparently smaller but nevertheless consistent with the measurements.

The new white dwarf velocity amplitudes are considerably lower than those initially established by Vennes & Thorstensen (1995). In low dispersion optical spectra of the white dwarf, the photospheric He II λ4686 absorption may be blended with chromospheric emission from the red dwarf. The GHRS data show no evidence of such contamination and are therefore entirely reliable.

Table 4 lists corrected and uncorrected orbital parameters of the three systems EUVE J0720−317, EUVE J1016−053, and EUVE J2013+400.

4.2. *White Dwarf Masses*

We now present a comparison between spectroscopic and gravitational mass measurements of the white dwarfs.

Spectroscopic Mass.—Figures 4*a* and 4*b* show new measurements of the photospheric helium abundance, effective temperature, and surface gravity of the white dwarfs in EUVE J1016−053 and EUVE J2013+400. We used line-blanketed hydrogen/helium model atmospheres in local thermodynamic equilibrium for comparison with earlier analyses. Table 5 summarizes available effective temperature and surface gravity measurements. We took a

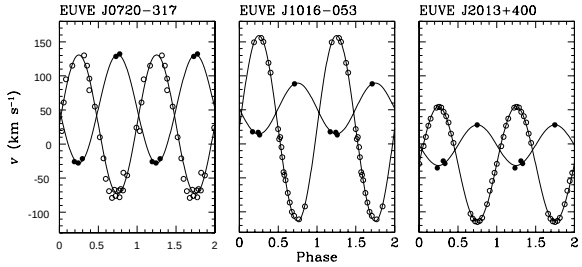

FIG. 3.—FUV (*filled circle*) and Hα (*open circle*) radial velocity measurements of, respectively, the white dwarf and the red dwarf along with best sinusoid fits (see Table 4). The red dwarf emission lines originate from upper atmospheric layers of the EUV-illuminated hemisphere and trace a lower orbit than absorption lines.

TABLE 5

WHITE DWARF TEMPERATURE AND GRAVITY

$T_{\rm eff}$ (10^3 K)	log g (cgs)	References
EUVE J0720−317		
53.5 ± 1.1.....	7.64 ± 0.10	1
52.4 ± 1.8.....	7.68 ± 0.10	2
55.1 ± 0.5.....	7.92 ± 0.04	3
53.0 ± 1.1.....	7.66 ± 0.07	Average of 1, 2
EUVE J1016−053		
56.4 ± 1.2.....	7.74 ± 0.07	4
54.8 ± 1.3.....	7.70 ± 0.10	5
55.0 ± 1.0.....	7.84 ± 0.10	6
55.4 ± 0.7.....	7.76 ± 0.05	Average of 4, 5, 6
EUVE J2013+400		
47.8 ± 2.4.....	7.69 ± 0.16	4
47.1 ± 1.0.....	7.74 ± 0.20	7
53.6 ± 1.1.....	7.67 ± 0.13	5
49.0 ± 0.7.....	7.65 ± 0.07	6
48.0 ± 0.9.....	7.69 ± 0.09	Average of 4, 6, 7

REFERENCES.—(1) Barstow et al. 1995b; (2) Vennes & Thorstensen 1996; (3) Finley, Koester, & Basri 1997; (4) Bergeron et al. 1994; (5) Vennes et al. 1997b; (6) this work; (7) Barstow et al. 1995a.

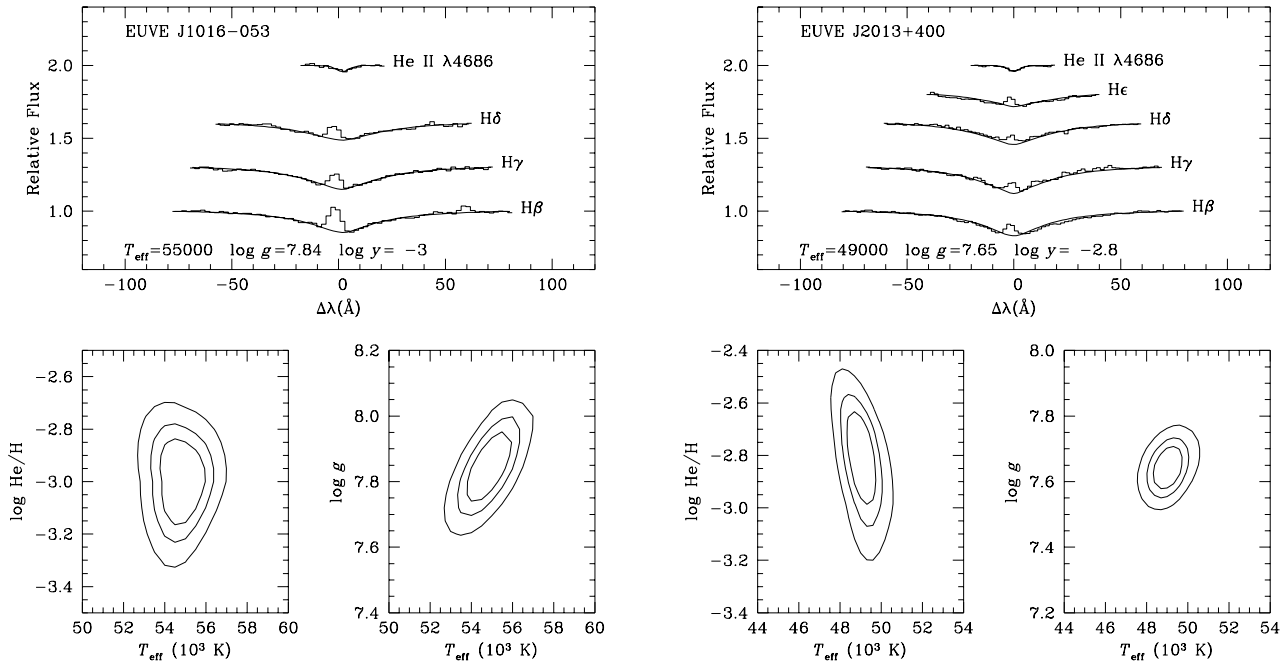

FIG. 4.—New parameter determinations ($T_{\rm eff}$, log g, He/H) for the white dwarfs EUVE J1016−053 and EUVE J2013+400 based on 1998 June Mount Stromlo and Sliding Springs spectroscopy and 1994 August Lick spectroscopy, respectively.

straight average of available measurements, excluding discrepant measurements of EUVE J0720−317 from Finley, Koester, & Basri (1997) and measurements of EUVE J2013+400 from Vennes et al. (1997b). Figure 5 illustrates our first set of constraints in the radius versus mass diagram. The area intersecting Wood's (1995) mass-radius relations (with and without hydrogen envelopes) and the surface gravity measurements is delineated with thick lines. Corresponding mass measurements and absolute luminosities, including the effects of uncertainties in temperature, are reported in Table 6.

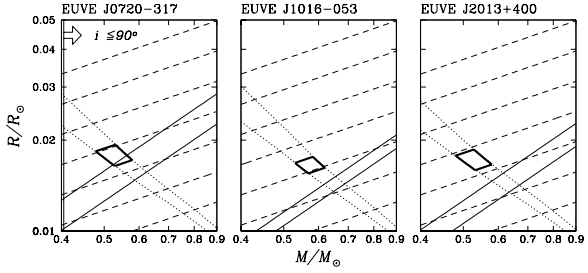

FIG. 5.—Three sets of constraints on the mass and radius of the white dwarfs: surface gravity (*diamonds*), gravitational redshift (*solid lines*), and Wood's (1995) mass-radius relations for carbon interiors and thick/thin hydrogen layers (*dotted lines*). Corresponding surface gravities at, from top to bottom, log g = 7.0, 7.2, 7.4, 7.6, 7.8, 8.0, and 8.2 are also displayed (*dashed lines*). Note the offset between masses and radii derived from the gravitational redshifts and the same quantities derived from the surface gravity measurements. Vennes & Thorstensen (1994a) noted a -4 km s^{-1} offset between systemic velocities defined by absorption and emission lines; corrections to the systemic velocities of the order of -4 to -6 km s^{-1} reduce the gravitational redshift measurements by the same amount and would restore consistency.

Gravitational Mass.—Taking at face value the systemic velocities obtained from Hα emission lines and interpreting the apparent redshift of white dwarf absorption lines as entirely due to the differential gravitational redshift—$\sim$0.5 versus $\sim$20–30 km s^{-1} for the dMe and the DA stars, respectively—we deduce a range of masses for the white dwarfs. Table 6 summarizes our new gravitational masses and corresponding absolute luminosities. Figure 5 shows that, with the exception of a slight overlap in the case of EUVE J0720−317, the gravitational masses are systematically higher than the spectroscopic masses. If we arbitrarily enforce a match between the surface gravity and the gravitational redshift measurements, we find that the white dwarfs *appear* to have larger radii and masses than predicted by Wood's (1995) mass-radius relations. However, systematic effects in radial velocity measurements offer a more likely explanation of the discrepancy. In fact, our new gravitational redshift measurements appear overestimated by $\sim$3 km s^{-1}. Vennes & Thorstensen (1994a) noted in the case of Feige 24 that the Hα velocities *may* underestimate the true systemic velocity, resulting in inflated estimates of

TABLE 6

WHITE DWARF MASSES, ABSOLUTE LUMINOSITIES, AND COOLING AGES

System	$M_{\rm sp.,thin}$[a] ($M_\odot$)	$M_{\rm sp.,thick}$[a] ($M_\odot$)	M_V[a] (mag)	Age[a] (Myr)	$M_{\rm GR,thin}$ ($M_\odot$)	$M_{\rm GR,thick}$ ($M_\odot$)	M_V (mag)
EUVE J0720−317.....	0.51 ± 0.03	0.57 ± 0.02	8.57 ± 0.19	1.8-2.4	0.56 ± 0.03	0.59 ± 0.03	8.86 ± 0.23
EUVE J1016−053.....	0.55 ± 0.02	0.60 ± 0.02	8.72 ± 0.14	1.6-2.1	0.63 ± 0.02	0.67 ± 0.02	9.06 ± 0.13
EUVE J2013+400.....	0.51 ± 0.04	0.56 ± 0.03	8.74 ± 0.21	2.4-3.2	0.61 ± 0.03	0.64 ± 0.03	9.16 ± 0.15

[a] Based on average spectroscopic values.

the white dwarf gravitational redshift. A radial velocity analysis of absorption features in the M-dwarf spectra would resolve the matter; relative faintness of the three red dwarfs would require the measurements to be obtained with a large-aperture telescope (greater than 3 m).

4.3. *System Inclinations*

Adopting the corrected mass functions (Table 4) and the full range of white dwarf spectroscopic masses (Table 6), we infer a range of system inclinations of $i \geq 62°$, $i = 55°$–$65°$, and $i = 31$–$37°$ for EUVE J0720−317, EUVE J1016−053, and EUVE J2013+400, respectively. The measurements are in agreement with observed Hα equivalent width variations, which, using Thorstensen et al.'s (1978) EUV-illumination model in the optically thin case (model A), imply relatively high inclinations for EUVE J0720−317 ($i \sim 57°$; Vennes & Thorstensen 1996) and EUVE J1016−053 ($\sim 55°$; Thorstensen et al. 1996), and a lower inclination for EUVE J2013+400 ($\sim 38°$; Thorstensen et al. 1994).

4.4. *Red Dwarf Masses*

Adopting spectroscopic white dwarf mass measurements and *corrected* mass ratios, we infer masses of $M_{\rm dMe} = 0.39 \pm 0.07$, 0.15 ± 0.02, and $0.18 \pm 0.04\ M_\odot$ for the companions of EUVE J0720−317, EUVE J1016−053, and EUVE J2013+400, respectively. Following Kirkpatrick, Henry, & McCarthy's (1991) mass versus spectral-type relation, the red dwarfs in EUVE J0720−317, EUVE J1016−053, and EUVE J2013+400 would belong to the ∼dM2, ∼dM5, and ∼dM4 spectral types, respectively, close to our own spectroscopic classifications.

4.5. *A Note on the Companion of EUVE J1016−053: Radial Velocity, Proper Motion, and Distance*

Jomaron et al. (1993) noted that EUVE J1016−053 has an M-type companion 3″.2 away (see Fig. 6). We will refer to the companion as EUVE J1016−053C and the DAO+dM binary as component A+B (AB) when needed.

Is the visual pair accidental? As noted earlier, the Hamilton echelle velocity of EUVE J1016−053C differs insignificantly from the systemic velocity of EUVE J1016−053AB inferred from the Hα orbit, which supports a physical association. We also measured the proper motions of AB and C by comparing direct CCD images obtained 1994 December 2 and 1997 December 15. The 1994 picture is described by Thorstensen et al. (1996); the 1997 picture was obtained with the 2.4 m telescope and a 2048^2 SITE CCD at 0″.275 pixel^{-1} in 0″.85 seeing. We measured image centroids using DAOphot (Stetson 1987) and determined the coordinate transformation between the pictures by fitting a linear six-constant plate model to 10 stars in common (excluding EUVE J1016−053 AB and C). The transformation had a rms residual of 50 mas, or 16 mas yr^{-1} for proper motion; this figure includes proper motions of the reference stars as well as all other sources of scatter. EUVE J1016−053 AB and C showed a strikingly large, common proper motion, much larger than any of the other stars in the field. The vector difference of the proper motions of AB and C was only 5 mas yr^{-1}, which is consistent with zero. The proper motion of AB and C (with respect to the reference stars used) is

$$\mu = 95 \text{ mas yr}^{-1} \quad \text{in P.A.} = 81 \pm 10° .$$

The common proper motion and radial velocity demonstrate that the pair is *not* accidental.

With the physical pairing established, we ask if the distance derived from parallax of the companion concurs with the distance derived from our white dwarf model.

The distance estimates make use of the colors and magnitudes given in Table 7. The 1994 December photometry is described by Thorstensen et al. (1996). The 1997 December data included the pictures used for the proper motion studies described earlier. Observations of numerous

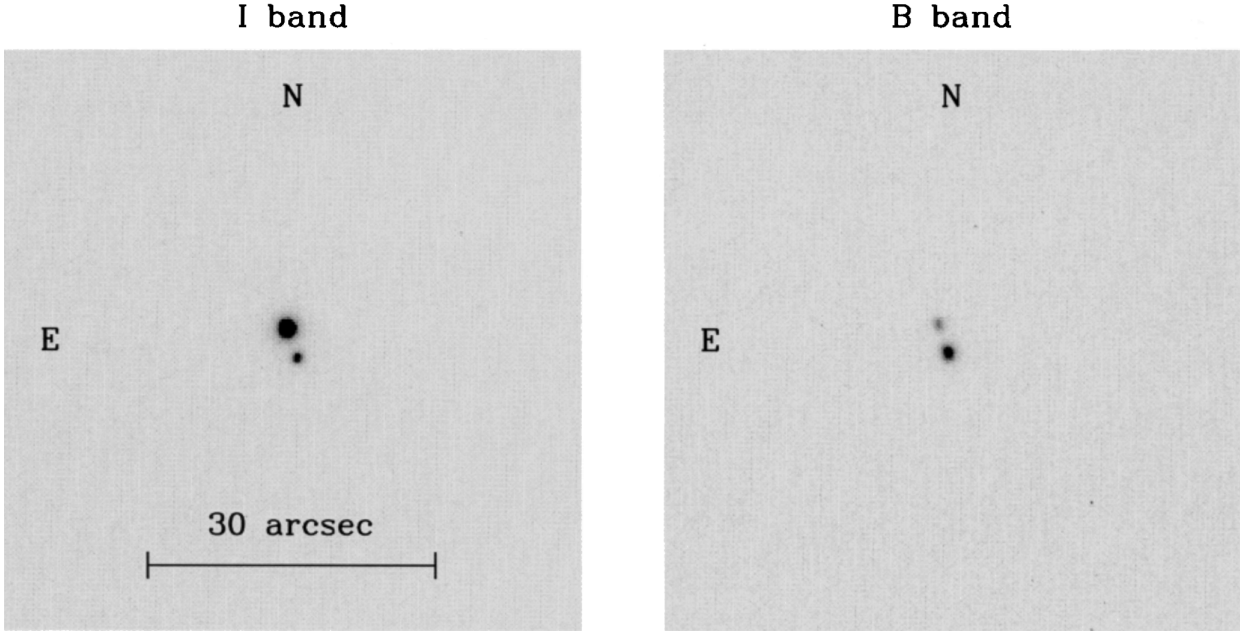

FIG. 6.—Near-infrared (*I*) and blue (*B*) MDM 2.4 m telescope images showing EUVE J1016−053 and, 3″.2 away, a nearby companion. Proper motion and radial velocity measurements suggest a physical association. We resolved a discrepancy in photometric distance estimates with the realization that the visual companion is a close dM+dM binary.

TABLE 7

PHOTOMETRY OF EUVE J1016−053

UT Date	Filter	Magnitude (AB)[a]	Magnitude (C)[a]
1994 Dec 2.55	V	14.15 ± 0.03	13.59 ± 0.03
	$B-V$	− 0.18 ± 0.04	+ 1.47 ± 0.04
	$V-R$	− 0.05 ± 0.04	+ 0.96 ± 0.05
1997 Dec 15.57.....	V	14.14 ± 0.02	13.59 ± 0.02
	$B-V$	− 0.24 ± 0.02	+ 1.51 ± 0.03
	$V-I$	− 0.05 ± 0.03	+ 1.92 ± 0.03
1997 Dec 16.56.....	V	14.14 ± 0.01	13.57 ± 0.01
	$B-V$	− 0.21 ± 0.02	+ 1.51 ± 0.02
	$V-R$	− 0.05 ± 0.02	+ 0.91 ± 0.02
	$V-I$	− 0.05 ± 0.02	+ 1.97 ± 0.02
(Adopted)	V	14.14 ± 0.02	13.58 ± 0.02
	$B-V$	− 0.21 ± 0.04	+ 1.50 ± 0.04
	$V-R$	− 0.05 ± 0.03	+ 0.92 ± 0.03
	$V-I$	− 0.05 ± 0.03	+ 1.95 ± 0.03
	$(R-I)$	0.00 ± 0.03	+ 1.03 ± 0.03

[a] Component AB is the close white dwarf/red dwarf binary; component C is the optical companion 3.″2 distant.

Landolt (1992) photometric standards on both nights yielded a transformation to the $UBV(RI)_{KC}$ system, the scatter of which suggested ∼0.02 mag uncertainties in the colors. A few of the standards observed were redder than EUVE J1016−053C. On both nights good seeing allowed DAOphot (Stetson 1987) to separate the contributions of the two components very cleanly.

Table 8 summarizes various distance estimates. The first two rows are based on our white dwarf model and include a small correction for the secondary contribution following Thorstensen et al. (1996). Subsequent entries, which we describe here in greater detail, refer to EUVE J1016−053C.

While we do not have our own classification spectrum of EUVE J1016−053C, we can estimate a spectral classification from the colors. To do this we determine a color-spectral type relation by comparing objects in common between Stauffer & Hartmann (1986), who give accurate colors, and Boeshaar (1976), who gives definitive classifications. This procedure yields M1.5 ± 0.5 (estimated error) for EUVE J1016−053C, and the third estimated distance in Table 8 follows from Boeshaar's spectral type–M_V relation. The uncertainty estimate includes the propagated uncertainty in the colors and assumes a 0.2 mag cosmic scatter in the main sequence (Upgren et al. 1997). Our Hamilton echelle spectrum corroborates the estimated spectral type, since the spectrum of EUVE J1016−053C appears very similar in overall appearance to that of Gliese 526, which Boeshaar classified as M1.5. Jomaron et al. (1993) estimate a dK8–dM1 classification, just consistent with our value.

The remaining entries in Table 8 invoke direct calibrations of the main-sequence color–absolute magnitude relation. Upgren et al. (1997) derive M_V–$(R-I)$ relations from *Hipparcos* parallaxes, and distinguish "old disk" and "young disk" relations. Patterson, Ianna, & Began (1998) derive an M_I–$(V-I)$ relation from nearby stars.

If EUVE J1016−053C is itself a single star, the direct calibrations of M versus color all give distances much less than derived from the white dwarf model. This discrepancy can be reduced (by up to 0.75 mag) if EUVE J1016−053C is itself a double, making the system *quadruple*. Our single Hamilton Echelle spectrum corroborates this interpretation; the lines appear broad, and on closer examination two sets of lines are just resolved. In the velocity analysis many of the echelle orders show two distinct cross-correlation peaks (Kurtz & Mink 1998) at the barycentric velocities + 17.3 ± 0.5 and +30.3 ± 0.5 km s^{-1}, which we now arbitrarily assign to components C and D, respectively. Further observations will be needed to determine the parameters of the second binary; the velocity separation suggests a period of months or years. The entries labeled "binary" in Table 8 have been adjusted to account for the apparent duplicity of EUVE J1016−053CD, assuming equal-brightness components.

Even after correcting for duplicity, EUVE J1016−053C is unexpectedly luminous; *all* the luminosity estimates suggest the distance is smaller than the distance derived from the white dwarf absolute luminosities, either based on spectroscopy or gravitational redshift measurements, although some of EUVE J1016−053CD's luminosity indicators are formally in agreement with the white dwarf luminosity based on the gravitational redshift. The estimates based on the *Hipparcos*-based results of Upgren et al. (1997) are the most discrepant, requiring over 1 mag of adjustment to bring about agreement.

5. NOTES ON EVOLUTIONARY PROSPECTS

We now examine evolutionary prospects for the three EUV-selected systems, following the work of King et al. (1994). For any values of the mass ratio, $q = M_2/M_1$, the

TABLE 8

DISTANCE ESTIMATES FOR EUVE J1016−053

Method	Reference	Implied M	Implied $m-M$
WD model (Spec.).....	1	M_V(WD) = 8.72 ± 0.14	5.48 ± 0.16
WD model (GR)	1	M_V(WD) = 9.06 ± 0.13	5.14 ± 0.15
m.s. M_V vs. sp	2	$M_V(B)$ = 9.6 ± 0.5	4.0 ± 0.5
Binary.....			4.8 ± 0.5
m.s. M_V vs. $R-I$.....	3	$M_V(B)$ = 10.7 ± 0.3	2.9 ± 0.3
Binary.....			3.7 ± 0.3
m.s. M_V vs. $R-I$.....	4	$M_V(B)$ = 11.3 ± 0.4	2.3 ± 0.4
Binary.....			3.0 ± 0.4
m.s. M_I vs. $V-I$	5	$M_I(B)$ = 7.6 ± 0.2	4.0 ± 0.2
Binary.....			4.8 ± 0.2

REFERENCES—(1) this work; (2)Stauffer & Hartmann 1986; Boeshaar 1976; (3) Upgren et al. 1997, for young disk population; (4) Upgren et al. 1997, for old disk population; (5) Patterson et al. 1998.

Roche lobe radius can be approximated by (Eggleton 1983)

$$R_{\mathrm{RL},2} = a \frac{0.49q^{2/3}}{0.6q^{2/3} + \ln(1 + q^{1/3})}, \quad (5)$$

where a is the orbital semimajor axis. Approximating the M dwarf radius with the theoretical ZAMS mass-radius relations of Eggleton, Fitchett, & Tout (1989), and using Kepler's third law, we then predict the contact period, P_{con}, corresponding to $R_2 = R_{\mathrm{RL},2}$. For a given pair (P_{orb}, P_{con}), King et al. (1994) predict the likely fate of a binary system. Our new mass and period measurements allow for a detailed comparison with these predictions.

EUVE J0720−137.—The relatively large mass of the secondary star ($M \sim 0.40\ M_\odot$) suggests that it is not fully convective, which may then induce magnetic braking and bring the system into contact. A comparison with the simulations of King et al. (1994) shows that the secondary will fill its Roche lobe within a Hubble time ($P_{\mathrm{con}} = 3.31$ hr), but because of its mass ratio ($M_2/M_1 \geq \frac{2}{3}$), it will also initiate unstable mass transfer.

EUVE J1016−053.—The secondary star in this system is near the low-mass end of the main sequence ($M \sim 0.15\ M_\odot$), consistent with the very low absolute luminosity estimated by Thorstensen et al. (1996). This system will not evolve as a bona fide cataclysmic variable ($P_{\mathrm{con}} = 1.75$ hr).

EUVE J2013+400.—We also find a low mass secondary in this binary ($M \sim 0.18\ M_\odot$), which then appears very similar to EUVE J1016−053; the secondary star will not fill its Roche lobe within a Hubble time either ($P_{\mathrm{con}} = 2.02$ hr).

In summary we find that the dM2 secondary star in EUVE J0720−317 will fill its Roche lobe and initiate unstable mass transfer, while the dM4-5 secondary stars in EUVE J1016−053 and EUVE J2013+400 will avert contact.

6. PROPER MOTIONS AND SPACE VELOCITIES OF EUVE 0720−317, EUVE J1016−053, AND EUVE 2013+400

We used two comparisons to determine proper motions of EUVE J0720−317 and EUVE J2013+400. First, as with EUVE J1016−053, we compared pairs of CCD images taken ~3 yr apart, the first epoch images being from the 1.3 m telescope and the second epoch being much larger scale images from the 2.4 m telescope. Second, we compared our 2.4 m images to the USNO-A2.0 catalog (Monet et al. 1998).[1] Even though the centering precision of the USNO-A2.0 is far worse than a CCD image, the USNO-A2.0 entries for these two targets are based on the first Palomar Sky Survey, so the elapsed time is greater than 40 yr. The proper motion accuracy of this second comparison was therefore slightly better than the CCD pairs. Because the second epoch material is common between the two determinations, they are not formally independent, but they are nearly so because the large-scale 2.4 m images contribute very little to the error budget. We again estimated uncertainties from the scatter of the reference stars (of which there were dozens at these low latitudes), so the reference star proper motions inflate the estimate of random uncertainties. The excellent agreement between the CCD pair and USNO/CCD determinations suggests that the quoted uncertainties are conservative. Table 9 details the proper motions.

The remainder of Table 9 gives calculations of the space velocities. We used systemic radial velocities from Table 4 and estimated M_V by averaging the results in Table 6; the uncertainties quoted for M_V are estimates of the external error. The apparent V magnitudes are from several sources. Vennes & Thorstensen (1994b) quote $V = 14.81$ for EUVE J0720−317, a value provided by M. Bessell and M. Dopita; our own CCD measurement from 1994 December agrees with this exactly. We could not find a V magnitude for EUVE 2013+400 in the literature, but CCD measurements from the 1.3 m telescope (1995 October) and the 2.4 m telescope (1997 September) both yielded $V = 14.02$. Neither of the nights was perfectly photometric and well calibrated, so this value is provisional, but it is probably accurate to ±0.05 mag. Spectrophotometry (Thorstensen et al. 1994) implies $V \sim 14.1$, corroborating the CCD measurements. The V magnitudes and uncertainties listed in Table 9 also include an estimate of the M-dwarf contribution. The space motions in Table 9 are in the Galactic system and have been adjusted to the local standard of rest (LSR) assuming a solar velocity $(u, v, w) = (-9, +12, +7)$ km s^{-1} with respect to the LSR (Mihalas & Binney 1981,

[1] EUVE J1016−053 does not appear in the USNO A catalogs, probably because the color difference and separation of the double star causes an apparent coordinate mismatch between the blue and red plates. The USNO catalogs include only images with matching detections on both the blue and red plates, and the matching radius is 2″.

TABLE 9

PROPER MOTIONS AND SPACE VELOCITIES

Parameter	EUVE J0720−317	EUVE J1016−053	EUVE 2013+400
Proper Motions:			
μ(CCD pairs; mas yr^{-1})	35 ± 10	95 ± 16	42 ± 7
θ(CCD pairs; deg)	270 ± 16	81 ± 10	31 ± 10
μ(CCD/USNO; mas yr^{-1})	36 ± 7	...	46 ± 12
θ(CCD/USNO; deg)	270 ± 11	...	42 ± 15
μ(adopted; mas yr^{-1})	36 ± 6	95 ± 16	43 ± 6
θ(adopted; deg)	270 ± 11	81 ± 10	34 ± 8
Distance Moduli:			
M_V (WD)	8.69 ± 0.25	8.90 ± 0.25	8.95 ± 0.25
V(WD)	15.0 ± 0.10	14.2 ± 0.05	14.15 ± 0.1
$m - M$	6.3 ± 0.3	(4.8 ± 0.4)	5.2 ± 0.3
Space Velocities:			
(u, v, w) (km s^{-1})	(+ 15, −4, −24)	(−33, + 8, + 48)	(+19, +36, +9)
Uncertainties (km s^{-1})	(6, 4, 7)	(10, 6, 8)	(5, 2, 3)

chap. 6). The uncertainties are based on a straightforward propagation of the errors in the relevant quantities; because the axes of (u, v, w) are not parallel to the plane of the sky, this procedure is not rigorous.

The system EUVE 1016−053 is kinematically unusual: the W component (perpendicular to the Galactic plane) is especially large. Upgren et al. (1997) give $\sigma_w = 12$ km s^{-1} for the young disk population and $\sigma_w = 31$ for the old disk, so the W component is anomalous for a young disk object. The discrepancy in absolute magnitude is smallest using the *young* population relation, yet the kinematics argue that the object is a member of the *old* disk population. Further kinematic studies of systems of this kind should be fruitful, because their distances and radial velocities can be determined quite accurately, compared with cataclysmic binaries. On the whole, the velocities suggest that the three precataclysmic systems are somewhat older than the youngest disk population.

7. WHITE DWARF COMPOSITION: ABUNDANCE OF HELIUM AND CARBON

The mixed hydrogen/helium atmosphere of some white dwarfs (DAO class) in the sample of close binaries may show the effects of accretion of material from the close companions. The presence of heavy elements in the atmospheres of the white dwarfs in EUVE J0720−317 and EUVE J1016−053 was inferred from a study of *EUVE* spectra of these objects (Dupuis, Vennes, & Bowyer 1997; Vennes et al. 1997a), but the detection of photospheric carbon in GHRS spectra of these two objects and of EUVE J2013+400 is the first direct evidence for the presence of photospheric heavy elements. Figures 7 and 8 show a model atmosphere analysis of the helium and carbon abundance in the three white dwarfs. We adopted the mean effective temperature and surface gravity measurements from Table 5 and computed detailed synthetic spectra containing variable carbon abundances (log C/H = −6.5, −6.0, −5.5, −5.0) based on a grid of H/He model atmospheres in local thermodynamic equilibrium. We adopted the Stark broadening calculations of Schoening & Butler (1989) for He II and the calculations of Dimitrijevic, Sahal-Brechot, & Bommier (1991) for C IV. Table 10 summarizes the abundance measurements along with published analyses.

Helium.—As suggested by Finley et al. (1997) the helium abundance in EUVE J0720−317 appears to have fallen by an order of magnitude circa 1996 September–1997 January relative to 1994 January–February. Dupuis et al. (1997) also measured an abundance of log He/H ∼ −4.5 based on a EUV spectrum obtained in 1995 December. The noted time variability may be evidence of episodic accretion with an increase of the helium abundance followed by a

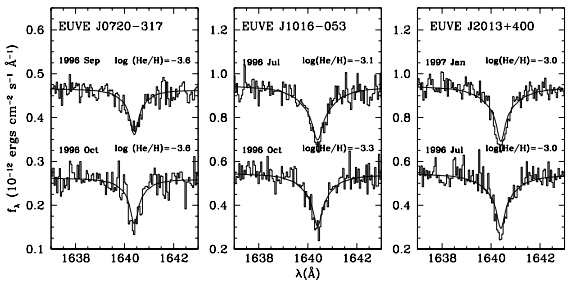

FIG. 7.—Model atmosphere fits to He II λ1640 line profiles in three white dwarfs. The GHRS spectra are binned by 3 pixels (∼0.05 Å). We used models with mean effective temperatures and surface gravities from Table 6. Upper spectra shifted upward by 0.2 (EUVE J0720−317) and 0.4×10^{-12} ergs cm^{-2} s^{-1} Å^{-1} (EUVE J1016−053, and EUVE J2013+400).

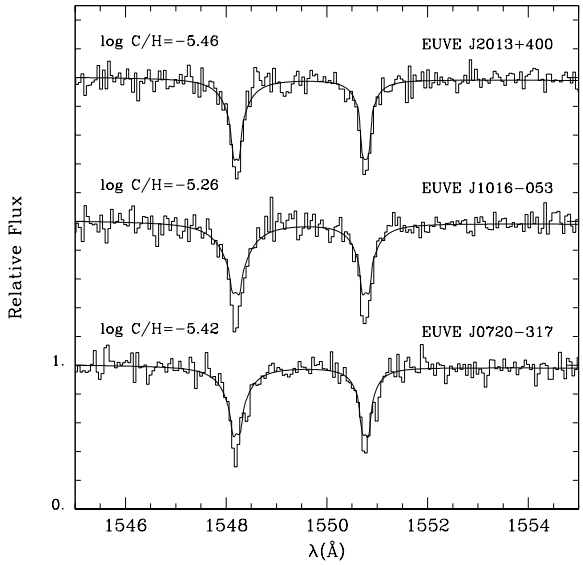

FIG. 8.—Model atmosphere fits to C IV λ1550 doublets in three white dwarfs. The GHRS spectra are binned by three pixels (∼0.05 Å). We used models with mean effective temperatures and surface gravities from Table 6 and *contemporary* helium abundances. Note a circumstellar component of the C IV doublet in EUVE J0720−317 at +17.8 ± 1.2 km s^{-1}.

TABLE 10

HELIUM AND CARBON ABUNDANCE

Date	log X/H	Line Measured	References
EUVE J0720−317			
1993 May.....	−3.47 ± 0.15	He II λ4686	1
1994 Jan	−2.60 ± 0.12	He II λ4686	2
1994 Feb	−2.72 ± 0.22	He II λ4686	1, 3
1996 Sep.....	−3.60 ± 0.10	He II λ1640	4
1996 Oct.....	−3.60 ± 0.12	He II λ1640	4
1997 Jan	≤ −3.4	He II λ4686	1
1996 Oct.....	−5.42 ± 0.08	C IV λ1550	4
EUVE J1016−053			
1992 Mar	−3.26 ± 0.22	He II λ4686	5
1994 Jan	−2.90 ± 0.12	He II λ4686	6
1996 Jul.....	−3.08 ± 0.10	He II λ1640	4
1996 Oct.....	−3.28 ± 0.08	He II λ1640	4
1998 Jun.....	−3.00 ± 0.15	He II λ4686	4
1996 Jul.....	−5.26 ± 0.11	C IV λ1550	4
EUVE J2013+400			
1992 Mar	−2.62 ± 0.63	He II λ4686	5
1992 Jul.....	−3.20 ± 0.40	He II λ4686	7
1994 Aug	−2.80 ± 0.15	He II λ4686	4
1994 Oct.....	−3.00 ± 0.20	He II λ4686	6
1996 Jul.....	−3.04 ± 0.10	He II λ1640	4
1997 Jan	−3.00 ± 0.08	He II λ1640	4
1997 Jan	−5.46 ± 0.07	C IV λ1550	4

REFERENCES—(1) Finley, Koester, & Basri 1997; (2) Vennes & Thorstensen 1996; (3) Barstow et al. 1995b; (4) this work; (5) Bergeron et al. 1994; (6) Vennes et al. 1997b; (7) Barstow et al. 1995a.

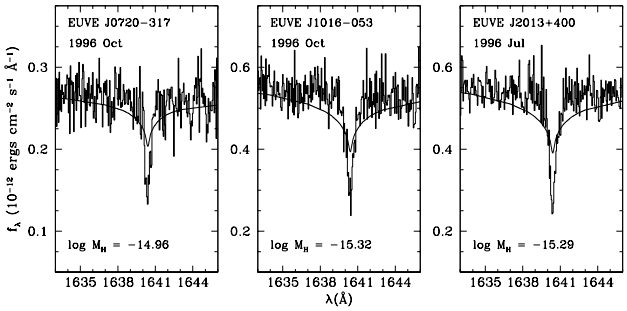

FIG. 9.—Same as Fig. 7, but using stratified model atmospheres from Vennes & Fontaine (1992). The fits are clearly unsatisfactory and rule out the presence of a pure diffusive equilibrium of hydrogen and helium in all three stars. We used models with mean effective temperatures and surface gravities from Table 6.

lapse of downward diffusion and chemical separation. The abundance of helium in EUVE J1016−053 and EUVE J2013+400 appears constant near log He/H ∼ −3. Figure 9 shows attempts at fitting the He II λ1640 line profiles with stratified model atmospheres from Vennes & Fontaine (1992). The hydrogen layer thickness would reach $\log M_H = -14.99 \pm 0.03$, -15.38 ± 0.06, and -15.35 ± 0.05 in EUVE J0720−317, EUVE J1016−053, and EUVE J2013+400, respectively. However, the broad-line wings and shallow-line cores from stratified models do not match the relatively narrow and deep He II line profiles observed in all three stars, showing that, contrary to the main postulate behind stratified model atmospheres, hydrogen and helium are not layered in a pure diffusive equilibrium and that the abundance of helium in the line-forming region is quasi-homogeneous (see Fig. 7). A similar conclusion was reached by Bergeron et al. (1994) based on optical He II λ4686 line profiles.

Carbon.—The presence of carbon in the atmosphere of EUVE J1016−053 has been noted in *IUE* high-dispersion spectra, but the low signal-to-noise ratio achieved in these exposures precluded a detailed abundance analysis (Thorstensen et al. 1996). On the other hand, Vennes et al. (1997a) and Dupuis et al. (1997) predicted an abundance of carbon of log C/H = −6.2 and −5.7 in EUVE J1016−053 and EUVE J0720−317, respectively, based on a study of the EUV continuum spectral energy distribution. GHRS spectra centered on the C IV λ1550 doublet were obtained at a single epoch for each star and reveal abundances of carbon *larger* than those inferred from EUV spectroscopy. Note also that although the C IV line wings are well reproduced, the predicted line cores are too shallow; LTE models may underestimate line core opacities relative to non-LTE models. Abundance estimates should not be affected. *HST* STIS spectroscopy of these objects should help establish a complete abundance pattern.

The presence of helium and carbon in large abundance, the variable helium abundance in EUVE J0720−317, and a fairly homogeneous distribution of helium throughout the atmospheres suggest on-going accretion of mass-loss material from the red dwarf companions.

8. SUMMARY

We have completed a series of optical and ultraviolet radial velocity measurements of the double-lined DAO+dM spectroscopic binaries EUVE J0720−317, EUVE J1016−053, and EUVE J2013+400. Our results imply a mass ratio close to unity for the binary EUVE J0720−317, which may come into contact within a Hubble time and initiate unstable mass transfer. The two other binaries will avert contact. Combining our results with the results of the radial velocity survey of Vennes, Christian, & Thorstensen (1998), we now identify six EUV-selected post-CE systems in EUV surveys—four dMe stars, one K star, and one A star—with secondary masses ranging from 0.15 to 1.8 $M_\odot$.[2]

With radial velocity and proper motion measurements we have established the kinematics of the three systems. EUVE J1016−053, in particular, has large velocity perpendicular to the Galactic plane, indicative of a older population. We have also determined that the white dwarf in EUVE J1016−053 is member of a quadruple system that comprises the close DA+dMe binary itself and a companion composed of two M dwarfs at a projected separation of ∼400 AU.

Finally, the atmospheric composition of the three white dwarfs show evidence of ongoing accretion from the red dwarf. The large carbon and helium abundance as well as long-term variations of the helium abundance in EUVE J0720−317 support the accretion model. The distribution of helium in the line-forming region also appears homogeneous as a function of depth. We also noted an inconsistency between spectroscopic mass (log g) and gravitational mass (γ_g) determinations which may be resolved with improved measurements of the binary systemic velocities. However, our main conclusions are not affected.

This research is supported by NASA grant NAG 5–2636 and by a Long Term Space Astrophysics grant to the University of California. S. V. is a QEII Fellow of the Australian Research Council.

[2] Initially identified as a close F+DA binary, the star HD 33959C now appears to be a triple system (R. Webbink 1998, private communication) with the yet unidentified third component being the close companion to the F star, and also a source of hard X-ray emission. Vennes et al.'s (1998) mass function requires a minimum mass of 0.25 $M_\odot$, which would be compatible with an active late-type star.

REFERENCES

Barstow, M. A., et al. 1995a, MNRAS, 272, 531
Barstow, M. A., O'Donoghue, D., Kilkenny, D., Burleigh, M. R., & Fleming, T. A. 1995b, MNRAS, 273, 711
Bergeron, P., Wesemael, F., Beauchamp, A., Wood., M. A., Lamontagne, R., Fontaine, G., & Liebert, J. 1994, ApJ, 432, 305
Boeshaar, P. C. 1976, Ph.D. thesis, Ohio State Univ.
Bowyer, S., Lampton, M., Lewis, J., Wu, X., Jelinsky, P., & Malina, R. F. 1996, ApJS, 102, 129
Catalán, M. S., Davey, S. C., Sarna, M. J., Smith, R. C., & Wood, J. H. 1994, MNRAS, 269, 879
Dimitrijevic, M. S., Sahal-Brechot, S., & Bommier, V. 1991, A&AS, 89, 581
Dupree, A. K., & Raymond, J. C. 1982, ApJ, 263, L63
Dupuis, J., Vennes, S., & Bowyer, S. 1997, in White Dwarfs, ed. I. Isern et al. (Dordrecht: Kluwer), 277
Eggleton, P. P. 1983, ApJ, 268, 368
Eggleton, P. P., Fitchett, M. J., & Tout, C. A. 1989, ApJ, 347, 998

Finley, D., Koester, D., & Basri, G. 1997, ApJ, 488, 375
Iben, I. Jr., & Livio, M. 1993, PASP, 105, 1373
Jomaron, C. M., Branduardi-Raymont, G., Bromage, G. E., Hassall, B. J. M., Hodgkin, S. T., Mason, K. O., Naylor, T., & Watson, M. G. 1993, MNRAS, 264, 219
Kelly, R. L. 1987, J. Phys. Chem. Ref. Data, 16, Suppl. 1
King, A. R., Kolb, U., de Kool, M., & Ritter, H. 1994, MNRAS, 269, 907
Kirkpatrick, J. D., Henry, T. J., & McCarthy, Jr., D. W. 1991, ApJS, 77, 417
Kurtz, M. J., & Mink, D. J. 1998, PASP, 110, 934
Landolt, A. U. 1992, AJ, 104, 340
Mihalas, D., & Binney, J. 1981, Galactic Astronomy (San Francisco: Freeman)
Monet, D., et al. 1996, USNO-SA2.0, (Washington DC: US Naval Observatory)
Nelson, B., & Young, A. 1970, PASP, 82, 699
Paczyński, B. 1976, in IAU Symp. 73: Structure and Evolution of Close Binary Systems, ed. P. Eggleton, S. Mitton, & J. Whelan (Dordrecht: Reidel), 75
Patterson, R. I., Ianna, P. A., & Begam, M. C. 1998, AJ, 115, 1648
Pye, J. P., et al. 1995, MNRAS, 274, 1165
Ritter, H., & Kolb, U. 1998, A&AS, 129, 83
Schneider, D. P., & Young, P. J. 1980, 238, 946
Schmidt, G. D., Smith, P. S., Harvey, D. A., & Grauer, A. D. 1995, AJ, 110, 398
Schoening, T., & Butler, K. 1989, A&AS, 78, 51
Shafter, A. W. 1983, ApJ, 267, 222
Stauffer, J. R., & Hartmann, L. W. 1986, ApJS, 61, 531
Stetson, P. B. 1987, PASP, 99, 191
Thorstensen, J. R., Charles, P. A., Bowyer, S., & Margon, B. 1978, ApJ, 223, 260
Thorstensen, J. R., Vennes, S., & Bowyer, S. 1996, ApJ, 457, 390
Thorstensen, J. R., Vennes, S., & Shambrook, A. 1994, AJ, 108, 1924
Tweedy, R. W., Holberg, J. B., Barstow, M. A., Bergeron, P., Grauer, A. D., Liebert, J., & Fleming, T. A. 1993, AJ, 105, 1938
Upgren, A. R., Ratnatunga, K. U., Casertano, S., & Weis, E. 1997, in *Hipparcos* Venice '97, ed. B. Battrick (Noordwijk: ESA), 583
Vennes, S., Christian, D. J., & Thorstensen, J. R. 1998, ApJ, 502, 763
Vennes, S., Dupuis, J., Bowyer, S., & Pradhan, A. K. 1997a, ApJ, 482, L73
Vennes, S., & Fontaine, G. 1992, ApJ, 401, 288
Vennes, S., Thejll, P., Génova-Galvan, R., & Dupuis, J. 1997b, ApJ, 480, 714
Vennes, S., & Thorstensen, J. R. 1994a, AJ, 108, 1881
———. 1994b, ApJ, 433, L29
———. 1995, in White Dwarfs, eds. D. Koester & K. Werner (Berlin: Spinger), 313
———. 1996, AJ, 112, 284
Wood, M. A. 1995, in White Dwarfs, ed. D. Koester & K. Werner (Berlin: Springer), 41